Materials Science-Poland, 40(1), 2022, pp. 84-100
http://www.materialsscience.pwr.wroc.pl/
DOI: 10.2478/msp-2022-0006

Fabrication and amplified spontaneous emission behavior of $FAPbBr_3$ perovskite quantum dots in solid polymer rods

M. Naziruddin Khan[1,*], Abdullah Almohammedi[1]

[1]Department of Physics, Faculty of Science, Islamic University, Madinah 42351, Saudi Arabia

Formamidinium lead tribromide ($FAPbBr_3$) perovskite quantum dot (PQ-Dot) solution was incorporated in a polymer sol, which was used to fabricate solid nanocomposite rods and disks. The solid nanocomposite samples were studied by different characterization techniques. The absorption, emission, and excitation spectra of the PQ-Dot in the solid rods/disks were quite significant as compared to the spectra of the PQ-Dot solution. Scanning electron microscopy (SEM) was used to inspect the structural morphology of the PQ-Dot in the solid environment. The PQ-Dot particles were evidently present in the solid matrix and were confirmed by the SEM images and energy dispersive X-ray spectroscopy (EDX) spectra. The size of the PQ-Dots was examined by transmission electron microscopy (TEM). The majority of the particles were about 3–8 nm in size. The spontaneous and stimulated emission profiles of the solid composite rods/disks were studied using pumping energy ranging from 2 μJ to 18 μJ from a high-power picosecond neodymium-doped yttrium aluminum garnet (Nd:YAG) tunable laser system. The observed emission signal was quite significant. The emission peak of the PQ-Dot solution had a slight change when it was included in the solid matrix. Amplified spontaneous emission (ASE) behavior was obtained from the PQ-Dot composite rod. The ASE peaks were quite steady at different levels of excitation energy. ASE was achieved at low threshold energy. The composite rod with ASE behavior indicates that it is a promising composite material that can be used to achieve lasing in the future. The ASE obtained from the composite rods/disks may improve to achieve lasing if a high concentration of PQ-Dot solution is used in the matrix.

Keywords: *perovskite quantum dot, composite rods/disks, absorption, emission, SEM, TEM, laser*

1. Introduction

In the past decade, organic light-emitting diodes (OLEDs) [1], LEDs [2], molecular organic devices [3], nanocrystals (NCs), and quantum-dot (Q-Dot) LEDs (QLEDs) [4] have been used as replacements for III–V semiconductors because they use high-vacuum and high-temperature processing materials. But the disadvantages of OLEDs include the following: they are prepared via vacuum-based sublimation and their processing is expensive. QLEDs have limited applications due to their high surface-defect concentration, which causes large nonradiative recombination [5]. Recently, hybrid (organic-inorganic) perovskite materials have found increasing applications in electronic and optoelectronic devices [6]. The shortcomings of III–V semiconductors and QLEDs are overcome in halide perovskites [7] and trihalide perovskite absorbers [8] due to the bright light of the organometal halide perovskite [9]. Moreover, halide perovskite materials have narrow emission line width, high quantum yield, direct bandgap, easily tunable bandgap, and high efficiency. The halide perovskite materials are cheap and are produced via facile synthesis using a solution-based process [10], overcoming efficiency limitations [11]. Therefore, they have emerged as materials with great potential for use in LEDs.

The basic structure of hybrid (organic-inorganic) perovskite has the same formula (ABX_3) as classical perovskites [6]. The crystalline structure of ABX_3 can form a 3D perovskite, with the organic cations A [methyl ammonium (MA) or formamidinium (FA)] [12] and B (an inorganic metal such as Pb or Cs), and X being a halogen (Cl, Br, or I; or mixed Cl/I, Br/I, or Cl/Br). These have emerged as materials used in solar cells [13]. Solid state principles have been applied to organic-inorganic perovskites [14]. Compared to the MA cation, the FA cation is reported to

* E-mail: mnkhan@iu.edu.sa

© Khan and Almohammedi 2022. This is an open access article distributed under the Creative Commons Attribution-NonCommercial-NoDerivatives 4.0 License. (http://creativecommons.org/licenses/by-nc-nd/4.0/)

be suitable for the octahedral cage, with much better thermal stability and photostability of the perovskite structure [15]. Moreover, FA does not have the tetragonal-to-cubic phase transition (as in the case for MA-based lead halide perovskite at ~50–60 °C), which can be an issue in relatively warm ambient conditions [16].

Over the past years, studies have been focused on the structural, optical, magnetic, quantum confinement, and dielectric properties of 2D layered perovskites, which yield strong exciton binding energies of up to ~300–400 meV [17]. Dyes have been incorporated in lead halide perovskite [18] because it is a promising material that has optoelectronic applications. Many works have been conducted on the different properties of 2D [19] and 3D [20] hybrid organic-inorganic perovskite materials. FA-based trihalide [21], stable inorganic–organic [22], and mixed Sn and Pb perovskites [23] have been studied. The electronic band could be tuned by changing the cation and anion in the perovskite lattice for solar cell applications [24].

The light emission of the organic-inorganic heterostructure using layered perovskite semiconductor [25], the electroluminescence of the quantum well structure [26] and heterostructure device [27] for emissive layered perovskite, LEDs [26], and lasing [28] has been reported. But, there are limitations to the practical applications of perovskite for LEDs because electroluminescence is obtained only at cryogenic temperatures. Moreover, halide perovskite-based thin film layers have been found to successfully emit light strongly at room temperature (RT) [9] and improve the efficiency of LEDs [29]. Many studies have been performed of different hybrid perovskite materials for use in efficient hybrid solar cells [30], photonic crystal laser [31], photonic source [32], conducting layered sheets [33], and LEDs [34]. Moreover, studies have been conducted on LEDs and photodetectors [35] using solution process hybrid organic-inorganic perovskite materials with high sensitivity [36], porous perovskite nanowires [37], and perovskite single crystal [38].

On the other hand, ultralow-threshold amplified spontaneous emission (ASE) at RT and lasing from perovskite polycrystalline thin films [7] has been observed. This has brought about a new direction of research on the light emission of 3D perovskites. Several groups have achieved ASE from different perovskite-based materials, such as solution-processed films [39], MA lead iodide [40], nanowires [41], and nanostructures [42]. Moreover, ASE of perovskite materials has been achieved using spherical resonators [43], flexible liquid crystal reflectors [44], and whispering gallery mode [45]. Lasing has been achieved in organo-lead halide microcrystal networks [46], and in-plane structuring of organic-inorganic perovskite films has been reported [47]. However, a high quality of halide perovskite and its composite matrix is still required for practical applications. The perovskite composite matrix is essential to enhance stable photoluminescence (PL) with large bandgap energy, long carrier lifetimes, and high carrier mobilities, in order to improve performance [48].

From the applications perspective, recently, perovskite quantum dot (PQ-Dot)-based solutions have emerged as a new class of materials. PQ-Dot is found to be stable, with high quantum yields, spectral broadening mechanism, and radiative decay of PL. Such properties are enhanced by crystal organometal halide perovskite [49], luminescent NC perovskite [50], and cesium lead halide perovskite [51]. Low-threshold ASE was attained from cesium lead halide-based solution [52], and solution films [53] showed improved stability [54]. ASE was achieved from different inorganic perovskite $CsPbBr_3$-based films [55]. Moreover, ASE was attained from phenylethylammonium (PEA)-based quasi-2D perovskite films [56] and from a single crystal of methylammonium lead bromide perovskite ($MAPbBr_3$) [57]. Lasing was achieved with cesium lead halide perovskite nanoplatelets [58] and self-assembled perovskite nanoparticles [59]. In addition, the optical and structural properties of PQ-Dots were reported [60]. Ultrastable stimulated emission from colloidal PQ-Dots was obtained [61]. Efficient and stable LEDs using PQ-Dots [62] and inorganic silica-coated PQ-Dots [63] were obtained. For enhanced stability, highly luminescent lead halide Q-Dots in hierarchical CaF_2 [64], luminescent lead bromide/$NaNO_3$ nanocomposite [65], and cesium lead halide Q-Dots in glass

[66] were studied. Ultrastable ASE was obtained from air-stable surface-passivated PQ-Dots [67]. ASE photostability was observed with cesium lead halide Q-Dots by applying a shorter capping ligand [68]. Though the optical properties of perovskite materials and Q-Dots have been significantly enhanced, there are some issues and drawbacks related to their chemical and thermal stability, photostability, and sensitivity to humidity or oxygen [69]. In humid environments, perovskite materials were reported to be unstable [70], and there were changes in their efficiency [71]. Evolution of the properties of cesium lead halide NCs was observed in an inert atmosphere [72], and their structure was degraded [73] in the ambient atmosphere. Moreover, to serve as a coherent laser source, PQ-Dots need to be stable in different environments. Based on the above considerations, significant works have been done to stabilize PQ-Dots/NCs in some environments such as polymer composite materials [41, 54]. The PQ-Dot/NC composite polymer materials could enhance the high stability of crystallinity in the host, the photophysical quality, and broad wavelength tunability. Majority of reported studies are either on solution processing perovskites [39, 54, 62] or PQ-Dot composite thin films [41, 54, 60]. Recently, incorporation of organo-silicon-coated $CsPbBr_3$ Q-Dots in polydimethylsiloxane was performed and PL enhancement was observed [74]. Cesium lead bromide Q-Dot was used in polymethylmethacrylate to improve its stability and maintain the optical properties [75].

To stabilize the PQ-Dots in an environment, the PQ-Dots solution needs to be doped or incorporated in matrices. This might extend their lifetime and protect them from humidity/moisture etc. PQ-Dots were successfully encapsulated or incorporated in silica [63], highly luminescent lead halide Q-Dots in hierarchical CaF_2 matrix [64], and luminescent lead bromide/$NaNO_3$ nanocomposite matrix [65]. Similarly, the optical properties [76] and structure of silicon NCs [77] in sol–gel matrix was studied, and significant, stable PL was observed. The morphology [78] and optical property of different types of colloidal porous silicon [79] doped in sol–gel matrices or oxide environments were studied, but this was not suitable for PQ-Dots due to the involvement of water.

To date, no attempt has been made to develop PQ-Dot polymer composite-based solid rods/disks/slab and so on using the doping process. Previously, we successfully fabricated silicon nanoparticle-composite polymer matrix and transformed it into nanocomposite rods. The optical properties of the dopants were significantly stable in ormosil matrix rod [80] and polymer matrix rod [81]. In this work, the PQ-Dot solution was directly encapsulated in a viscous polymer sol. The PQ-Dot composite sol was developed into the shape of rods/disks for the first time. A systematic study of the composite rods/disks was carried out using different optical characterization techniques. The optical properties, such as absorption, emission, spontaneous emission, and structural morphology, of the rod samples are discussed. The ASE-like spectra obtained from the composite rods are briefly discussed.

2. Materials and Q-Dots

The methyl methacrylate (MMA) monomer used in the present work was obtained from Aldrich. MMA is of analytical grade and thus free from inhibitor. Benzoylperoxide (BPO) obtained from Aldrich was used as an initiator to react in the polymerization process. The PQ-Dots (formamidinium lead tribromide [$FAPbBr_3$]) core solution in toluene at a concentration of 10 mg/mL and density of 0.87 mg/mL was bought from Quantum Solutions LLC, King Abdullah University of Science and Technology (KAUST), Thuwal, KSA. It contains PQ-Dot core and capping ligand of oleic acid and octylamine.

2.1. Preparation method

Before preparation, the MMA monomer was free from inhibitor; dilute sodium hydroxide was used with about 3%–5% of monomer. The compositions of reaction were as follows: initially, 40 mL of MMA was taken with 0.0300 g of initiator (BPO) to polymerize the monomer solution. The sol was stirred and allowed to polymerize at about 55–60°C to obtain the viscous phase. A known vol-

ume of PQ-Dot solution was added into the viscous solution and then stirred continuously for about 5–10 min to form the homogeneous solution. The ratio of PQ-Dot solution to polymer sol was about 1:1.5 or 1.5:2. The final composite solution was transferred into glass test tubes and smaller glass disks to form rods and disks, respectively. The tubes containing the solution were kept in an oven at 55–60°C for a week. After 1 week, the PQ-Dot composite polymer rods/disks formed solid samples and then were removed from the tubes/disks.

2.2. Characterizations

The optical properties of PQ-Dot solution and solid polymer composite samples were investigated. The absorption, emission, and excitation spectra of the samples were recorded in ultraviolet-visible-near infrared (UV-VIS-NIR) spectrophotometer (Model 670; JASCO, Japan) and Lumina fluorescence spectrophotometer (Thermo Scientific, USA). The surface morphology and particle size of the PQ-Dot solution and polymer matrix were inspected by field emission scanning electron microscopy (FESEM) (JSM-7500F; JEOL, Japan) and transmission electron microscopy (TEM) (JEM- 2100F; JEOL). The PQ-Dot solution and solid composite rods/disks were exposed to a UV lamp (EL series, 97620-42; Cole Parmer, USA) to check the light being emitted. The PQ-Dot composite polymer rods were cut and polished using a diamond cutting machine (Model 650; South Bay Technology, Inc., USA) and lapping and polishing machine (Model 920; South Bay Technology, Inc., USA). The samples were 5 mm × 5 mm in length. To study the spontaneous emission and ASE properties, 355-nm, 420-nm, 450-nm, and 465-nm laser sources of a high-power Q-Switched neodymium-doped yttrium aluminum garnet (Nd:YAG) picosecond tunable laser system (LS-2151, LOTIS TII) and optical parametric generator (OPG) were used. The pulse duration and repetition rate of the fundamental laser beam were 70–80 ps and 15 Hz, respectively. The maximum output energy of the 355-nm laser source was 21 mJ per pulse at 15 Hz. The output pump energy ranging from 2 μJ to 18 μJ per pulse was used for the target samples. The same geometry of measurement was set up for all samples. The samples were placed at the same position and subjected to transverse pumping. The laser beam was incident on the horizontal surface (length of rod) of rods and the diameter side of disk. The spontaneous emission signal from samples was monitored from the side of samples through an optical fiber of a spectrograph (QE65 Pro; Ocean Optics, USA) with and without collimating lens. Different lengths of the PQ-Dot composite polymer rods were cut and used for the ASE test. The size of the rods before they were cut was as follows: about 10 mm diameter and 40 mm length. After cutting the rods, the size was as follows: about 10 mm diameter × 5 mm, 3 mm, and 2 mm length. The diameter of the disk was 20 mm × 3 mm thickness.

3. Results and discussion

The PQ-Dot solution is directly embedded in the viscous polymer sol, which was used to fabricate the stable PQ-Dot solid composite cylindrical rods and disks. Fabrication and development of the solid composite samples were dependent on the factors of viscous phase solution, the timing of doping, temperature, and aging of the samples. The digital images of the PQ-Dot solution and composite polymer rod/disk under UV exposure are displayed in Figures 1A and 1B. Figures 1C and 1D show the composite rods before and after they were cut into different sizes. It is observed that the emission light of the composite rods is quite significant compared to that of the PQ-Dot solution. The significant emission from the composite rods/disk indicates that PQ-Dots can be encapsulated in polymer sol and developed into solid composite rods/disks. The composite rods could be easily cut and polished without harming the samples, as displayed in Figures 1C and 1D. To investigate the optical and structural properties of PQ-Dots in the solid polymer rods/disks, the samples were studied by different characterization techniques such as UV-VIS spectrophotometry, luminescence spectrophotometry, tunable lasing, and FESEM.

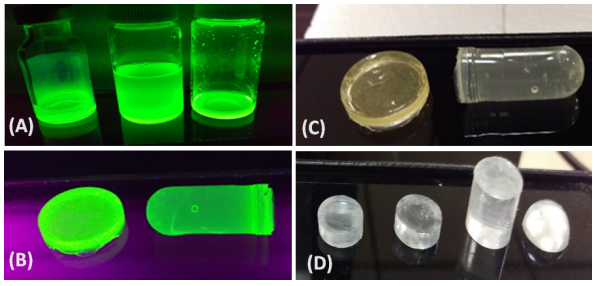


Fig. 1. Digital images of samples **(A)** PQ-Dot solution; **(B)** PQ-Dot solid composite polymer rods and disks exposed to ultraviolet lamp; **(C and D)** PQ-Dot composite rods before and after cutting the rods

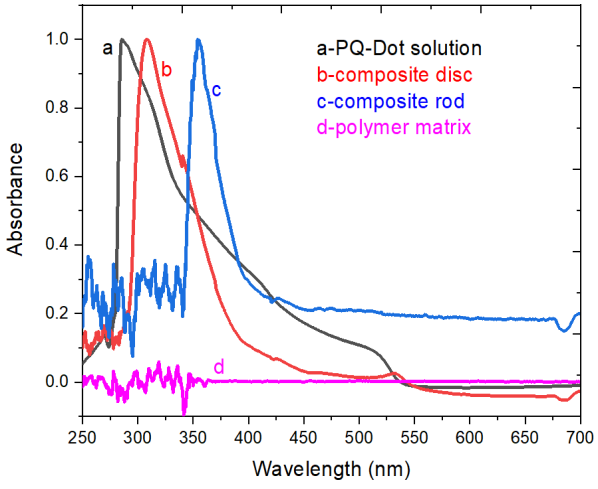


Fig. 2. Absorption spectra of PQ-Dots: (a) solution; (b, c) composite solid samples; and (d) polymer matrix

3.1. Absorption spectra

The UV-VIS absorption spectra of the PQ-Dot solution and solid composite rods/disks were recorded within the spectral range of 300–900 nm. The rods were put vertically in the sample compartment to facilitate the beam passing through the surface. The size of the reference sample was the same as that of the undoped rod. The direction of optical path of the disk was the side of the diameter surface. The normalized absorption spectra of both PQ-Dot solution and composite rod/disk are compared, as displayed in Figure 2(line graphs a–c). There are significant changes in the UV-VIS absorption spectra of the PQ-Dots in the solid polymer in relation to the absorption spectra of the PQ-Dot solution. But, the absorption peaks of the PQ-Dots in the polymer rod and disk appear within the spectral region of the PQ-Dot solution. The absorption spectrum is affected in the polymer matrix due to the influence of the solid environment. The absorption peak of the PQ-Dot composite rod is slightly different from that of the PQ-Dot composite disk due to the effect of the site of the samples. No doubt, the bandwidth and the absorbance of the PQ-Dot composite matrix were influenced by the solid matrix. Moreover, there could be an interaction between the PQ-Dot particles and the matrix environment. This could cause scattering, which has an effect on the absorption spectra, as shown in Figure 2(line graphs b and c). The observed absorption peaks of the PQ-Dot composite solid rod/disk are significant compared to the absorption peak of the PQ-Dot solution, as displayed in Figure 2. But the absorbance of PQ-Dots was reduced in the same spectral region.

The advantage of the composite polymer rods and disks over the composite films is that diverse shapes of samples with different concentrations of PQ-Dots in the matrix can be fabricated. These composite samples could be used to test for ASE. Indeed, the use of high concentration of PQ-Dots to prepare thin film-based sample with optical stability is also a challenge. Therefore, composite rods or disks may be easily fabricated with high concentration of PQ-Dots to improve the stability of Q-Dots and better protect them from oxygen.

3.2. PL property

The key interest of the present study is to stabilize the emission spectra of PQ-Dots in the environment of solid composite rods or disks, which could then be used to achieve ASE and lasing for potential applications. For this purpose, the emission property of PQ-Dots and its effect in solid rod and disk samples were studied. The emission spectra of the PQ-Dot solution and the composite rods/disks are shown in Figures 3A–3C. To verify the excitation wavelength of the samples at which a pumping laser source is to be used, different excitation wavelengths were selected. The samples were

Table 1. Comparison of the emission, excitation, spontaneous emission, and ASE maxima among the solution, composite rod, and composite disk

Sample	Emission maxima	Excitation maxima	Emission maxima excited by laser source	ASE maxima excited by laser
Solution	541 nm	355 nm, 375 nm, 416 nm, 463 nm	534 nm	556 nm
Composite rod	535 nm	390 nm, 410 nm, 461 nm	542 nm	
Composite disk	536 nm	310 nm, 370 nm, 412 nm, 461 nm	538 nm	

ASE, amplified spontaneous emission

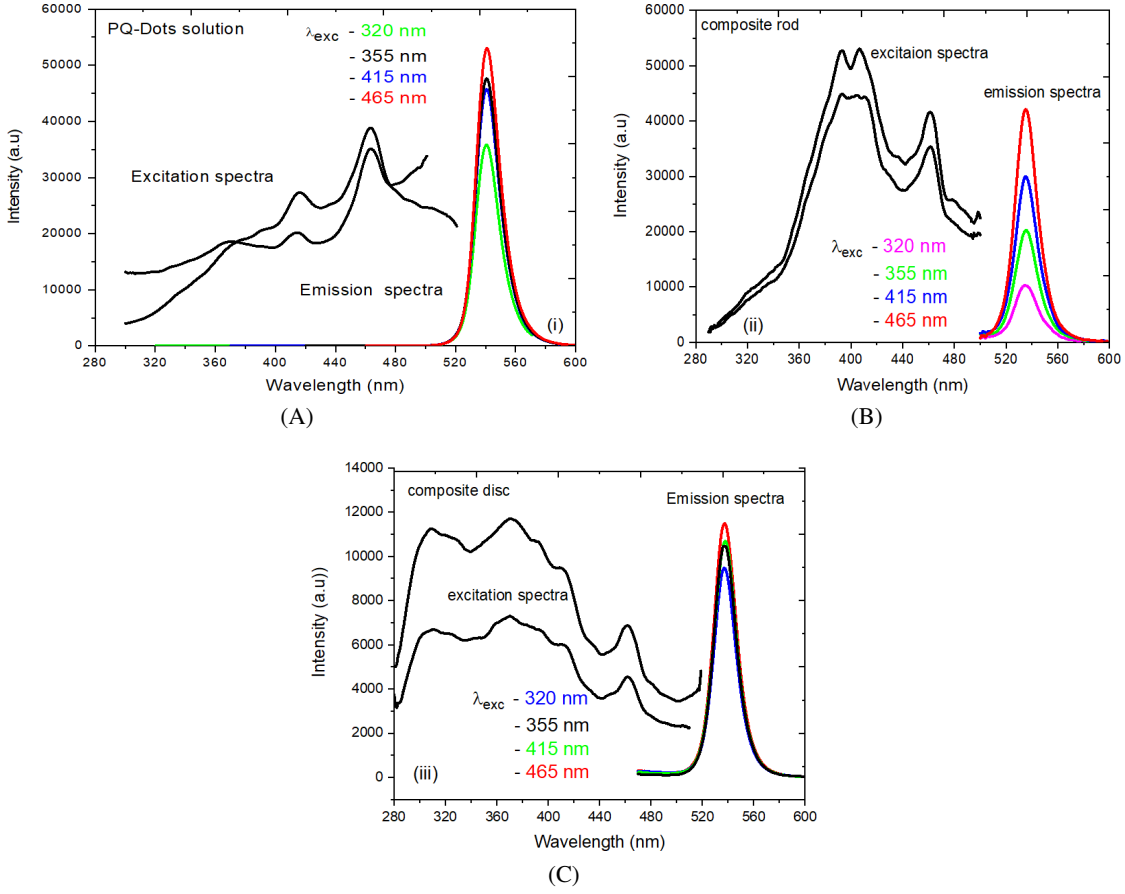


Fig. 3. Emission and excitation spectra of PQ-Dots excited at different wavelengths: **(A)** solution; **(B)** composite rod; and **(C)** composite disk

excited at 320 nm, 355 nm, 415 nm, and 465 nm, which corresponded to the absorption region of the PQ-Dots, as shown in Figure 2. Indeed, the emission intensity of PQ-Dots depends on the excitation wavelength. It is observed that the emission peaks of the PQ-Dots are stable, but the intensities change when the excitation wavelength changes. For instance, the emission and excitation spectra of the PQ-Dot solution are shown in Figure 3A. There was no shift in the positions of the emission peak when the different samples were excited at 320 nm, 355 nm, 415 nm, and 465 nm; only the corresponding relative intensities changed. Similarly, the corresponding excitation peaks of the PQ-Dots are not

changed, but a slight effect is found in the intensities, as shown in Figure 3A and Table 1. The emission peak of the PQ-Dot solution is at the center of about 542 nm. Changes in the emission intensities may be attributed to the different excitation energies. The PQ-Dot composite solid polymer rod and disk and the PQ-Dot solution were studied under the same conditions to study the effect of their emission spectra. The emission spectra of the PQ-Dot composites rod and disk are shown in Figures 3B and 3C.

The emission intensities of the PQ-Dot composite rod and disk are dependent on the excitation wavelengths but are stable at their corresponding peak positions. The emission peaks of the PQ-Dots in the rods and disks are at the center of 535 nm and 538 nm, respectively. A slight shift in peak position is observed, which may be due to the different distributions of the Q-Dots and sizes in the rods and disks.

Indeed, there is a significant shift in the emission and excitation peaks of the composite rods and disks compared to the emission peaks of PQ-Dots in solution. This may be due to the change from a solution medium to a solid environment. As seen in Table 1, the shifting of the emission peak positions in both PQ-Dot solution and solid composite rods/disks is not much large, but the change in intensity is quite significant, as shown in Figure 4. But the obtained emission signal from the solid composite matrix is quite significant compared to the emission of the PQ-Dot solution, indicating that there is proper distribution and interaction with the environment of the solid polymer rods.

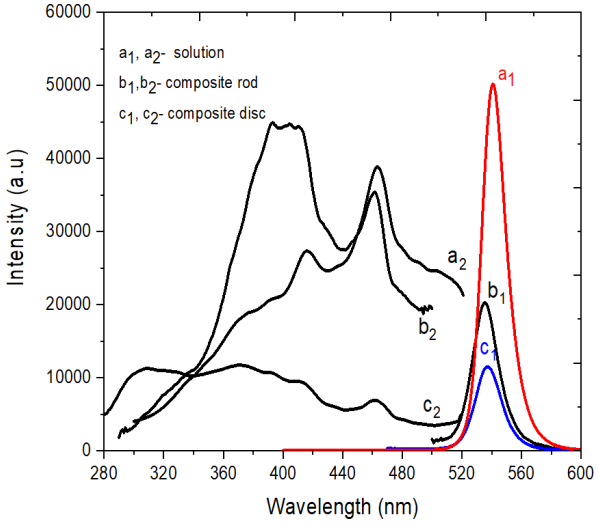


Fig. 4. Comparison of emission and excitation spectra of the PQ-Dot solution, composite polymer rods, and composite disks

The comparison of the emission and excitation spectra between PQ-Dot solution and composite solid is shown in Figure 4. The observed emission peaks a_1, b_1, and c_1 correspond to their excitation spectra a_2, b_2, and c_2, respectively. The excitation peaks of the PQ-Dot solution noticeably changed when the PQ-Dots were deposited in the solid matrix. As clearly seen in Figure 4, the emission and excitation peaks are influenced by the solid matrix.

3.3. Spontaneous emission and ASE spectra

The spontaneous emission spectra of the PQ-Dot solution, composite polymer rods and disks were studied, and the ASE condition was examined at 355 nm, 420 nm, 450 nm, and 465 nm using an exciting laser source of a high-power tunable picosecond laser system. Different low energies of all laser sources were used. The spontaneous emission spectra of the PQ-Dot solution composite polymer rods and disks excited by the 355-nm laser source at different energies are shown in Figures 5A and 5B. The observed peak of the composite at 534 nm slightly shifted from the relative emission peak of the PQ-Dot solution at 541 nm, as seen in Table 1. But, the corresponding intensities are influenced by the pumping energy; for instance, when the laser pump energy increases from 2 μJ to 8 μJ, the intensity of the PQ-Dot solution inclines, as shown in Figure 5A.

The solid composite rods and disks were fixed at the same geometrical position and pumped using the same excitation source and energy. The spontaneous emission signals obtained from both solid samples are significant, but their intensity is influenced by the pumping energy, as shown in Figure 5B. The comparison of the spontaneous emission spectra of the PQ-Dot solution, composite solid rod, and composite disk is displayed in Fig-

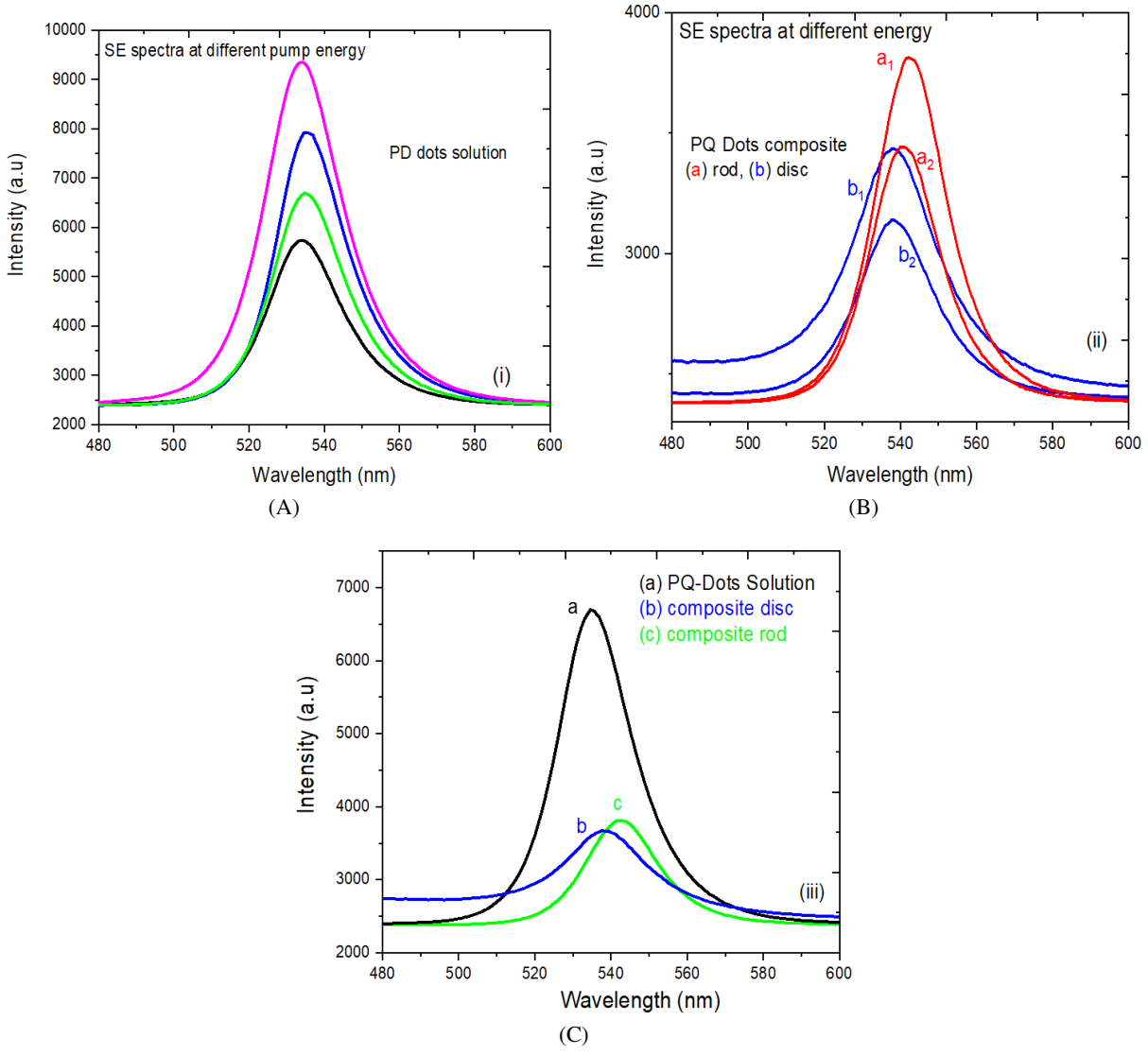


Fig. 5. Spontaneous emission (SE) spectra of **(A)** PQ-Dot solution, **(B)** cylindrical composite rod and disk, and **(C)** the difference between the conditions for registration of the spectra

ure 5C. The positions of the spontaneous emission peaks of the PQ-Dots in the solid matrix significantly changed compared to the spontaneous emission of the PQ-Dot solution, as given in Table 1. This effect could be attributed to the site effect of the solid matrix when the laser beam is incident on the sample surface. Further, the spontaneous emission intensity is quite improved and increases when a cylindrical focusing lens is used. The comparison of the spontaneous emission spectra of the composite rod with and without a focusing lens is shown in Figure 5D. Increasing intensity of spontaneous emission with the solid samples indicates that a proper optical geometry and a different size of the solid sample will also help to achieve ASE and lasing.

In fact, the spontaneous emission intensities of the PQ-Dot composite are generally dependent on the geometrical setup of the samples in relation with the pumping source. The composite rod was 10 mm in diameter and 40 mm in length. Therefore, different sizes of the rod were cut into differ-

ent lengths, and the ASE property was tested by using different laser sources and energies under the same condition. The exciting laser sources were selected as 355 nm, 420 nm, 450 nm, and 465 nm based on the absorption region.

Three laser sources (420 nm, 450 nm, and 465 nm) were excited with the OPG) system. The comparison of the spontaneous emission spectra observed from the different excitation laser sources is displayed in Figure 6A. The spontaneous emission spectra of the rod are noticeably narrowed with increase in intensity when it was excited by the 465-nm laser source. A relative shift in peak positions is obtained at excitation wavelengths of 355 nm, 420 nm, and 450 nm, respectively. The obtained narrow bandwidth and intensity of the spontaneous emission spectra excited by 465 nm seem to exhibit stimulated emission.

The spontaneous emission spectra are influenced by the size and length of rods as shown in Figure 6B. The peaks and intensity of the short composite rod are stronger than those of the longer rod. This indicates that the spontaneous emission property of the PQ-Dots depends on the thickness of the composite sample. The shifting of the spontaneous emission peaks is within the range of 10 nm, as displayed in Figures 5C and 5D, Figures 6A and 6B, and Table 1.

The present observation shows that the spontaneous emission signal is substantially influenced by various parameters, such as excitation wavelengths, shape, and size, along with the geometrical position of the composite samples. But a different concentration-based composite sample with diverse shape, size, and geometrical position of samples will be helpful to explain the ASE condition. As seen in Figure 6B, the light emitted from the shorter rod (10 mm × 5 mm) under UV exposure is quite strong compared to that from the longer one (10 mm × 40 mm). Accordingly, the evolution from spontaneous to stimulated emission for the shorter rod sample was detected when it was excited at 465 nm. The change of relative peaks may be due to the effect of the samples' site in relation with the laser source. Moreover, the emission of the rods shows that PQ-Dots were well distributed, without aggregation of particles in the solid environment.

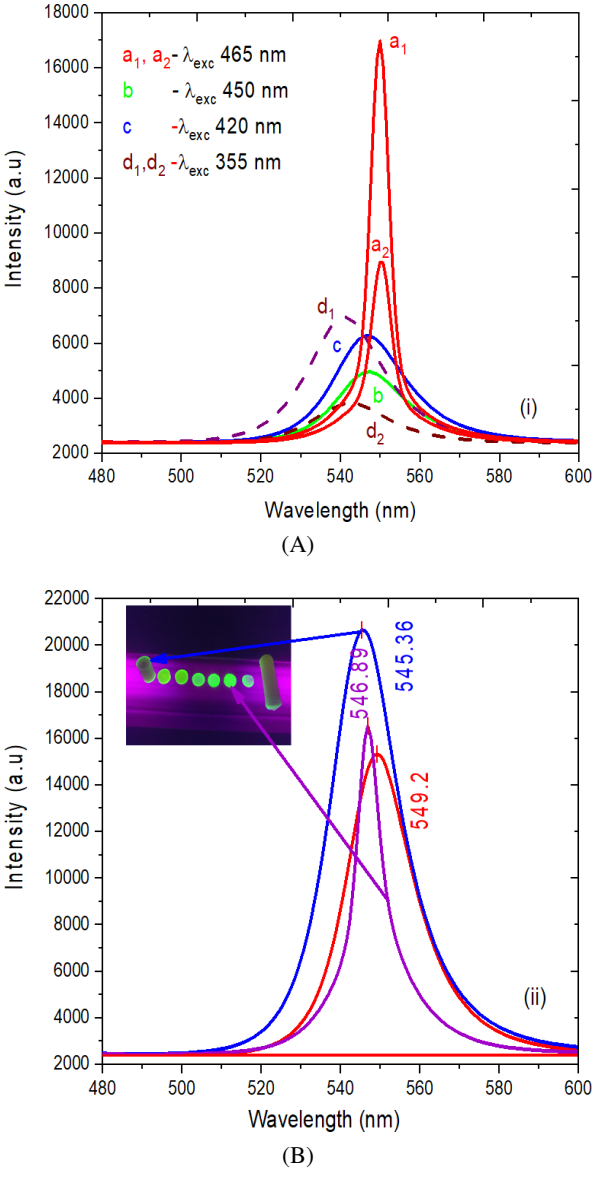


Fig. 6. Comparison between spontaneous and stimulated emission spectra of perovskite quantum dot composite rods at different **(A)** 465 nm excitation wavelengths and **(B)** sample sizes

Therefore, the inclining of emission intensity from the shorter rod may correspond to the emission behavior of the PQ-Dot composite thin film since ASE was far from the edge surface of the perovskite films [42, 55, 60, 63, 64]. It may be that when a laser beam is incident on a small-sized sample, the maximum area of the sample could enhance the emission. When the beam falls and concentrates

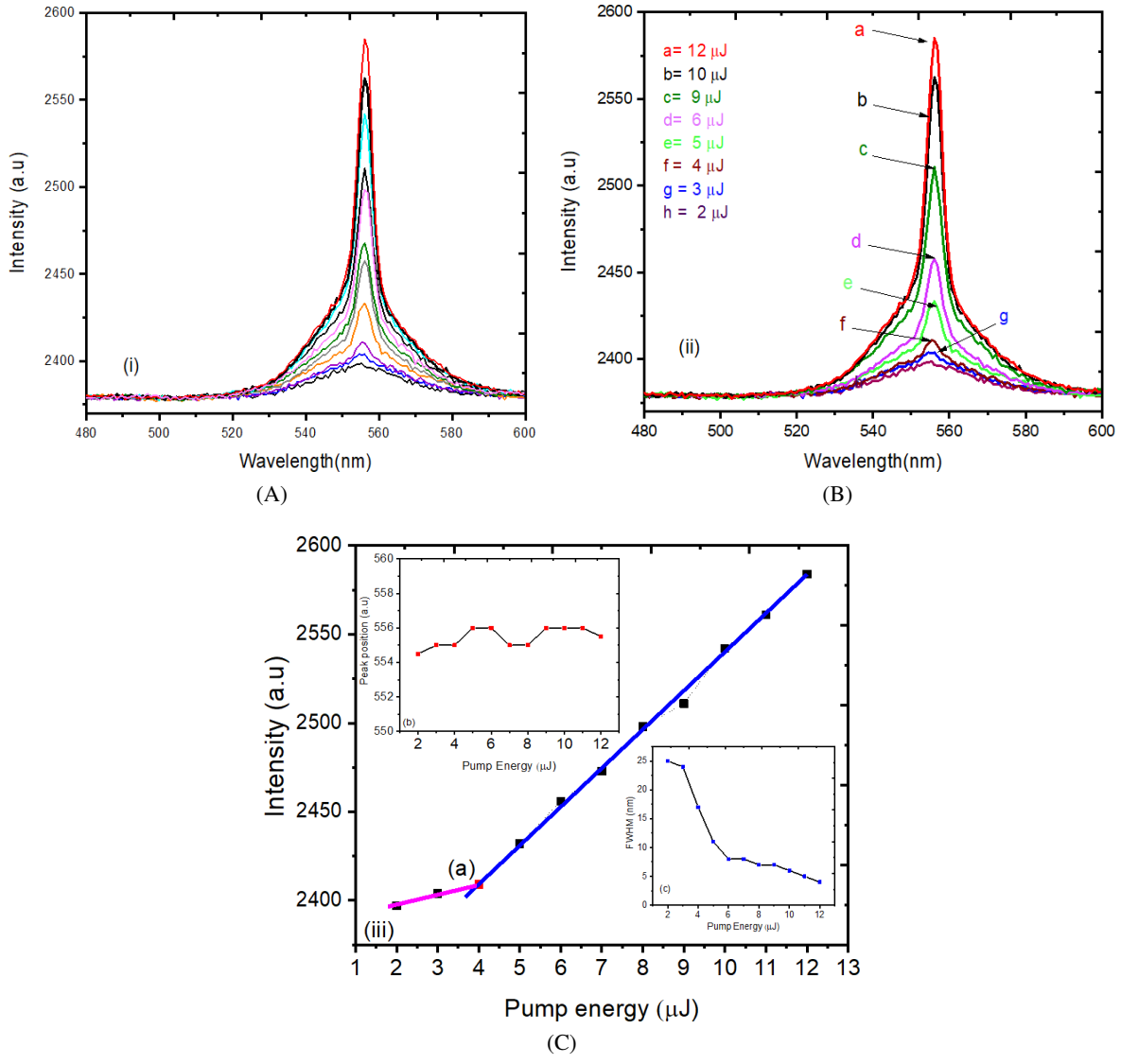


Fig. 7. **(A, B)** ASE behavior spectra; **(C)** (a) threshold line, (b) peaks, and (c) FWHM with 465-nm pump energy of perovskite quantum dot composite rod. ASE, amplified spontaneous emission; FWHM, full width at half maximum

on a small area of the sample surface, it may exhibit strong emission. In fact, the key issue of composite thin films on substrates is their instability in environments and surfaces.

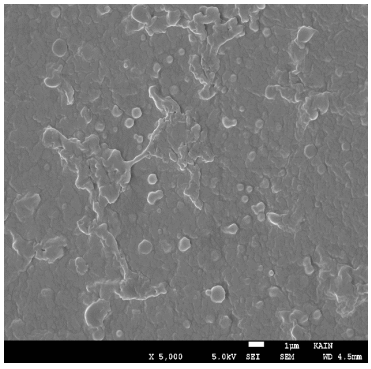
The stability problem of composite films can be reduced by using the composite rod or disk because the PQ-Dots inside the rod will be able to protect its oxide environment. Moreover, the composite rod was assessed repeatedly for many days, during which no photobleaching on the surface of the composite rod or disk was seen (not detailed here). In the present observation, the ASE condition was achieved at low pumping energy, which reduced the photobleaching on the composite rods or disks.

From the above viewpoint, the size of the composite rods after they were cut was about 10 mm diameter × 5 mm, 3 mm, and 2 mm length, as shown in Figure 6B. These rods were examined by pumping 465 nm laser sources at different low energies.

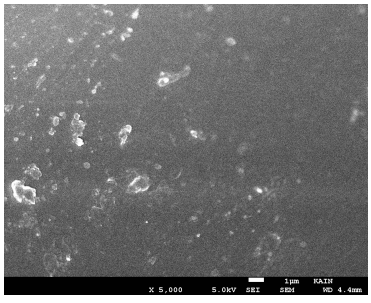
The pump energy used was from 2 μJ to 18 μJ. Interestingly, when the low excitation energy was pumped on the rod sample through a cylindrical lens, ASE-like spectra were detected, as shown in Figure 7A. When the 465 nm laser source at different energies was used for pumping of the samples, a clear change of the bandwidth and relative intensity was observed. The relative intensity increases exponentially as the excitation energy increases, as shown in Figures 7A and 7B. As the excitation energy increases from 4 μJ to 5 μJ, the intensity sharply increases with narrowing bandwidth.

The full width at half maximum (FWHM) is changed when the pump energy applied is changed from 2 μJ to 4 μJ. The lowest narrow bandwidth is detected when the pumping energies used are from 5 μJ to 12 μJ, and the observed features are ASE-like spectra, as noted in Figure 7A. The ASE is achieved with a threshold energy of 4 μJ/cm^2, as shown Figure 7C-a.

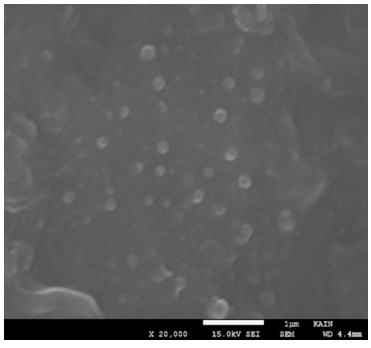
The FWHM of the ASE spectra decreases as the energy increases from 2 μJ to 6 μJ. Lower FWHM is obtained when pumping energy between 7 μJ and 12 μJ is used. No significant shift of peaks is observed when the excitation energy changes, as shown in Figure 7B. The intensity of the ASE peak exponentially inclines with increase in the energy from 5 μJ to 12 μJ, as plotted in Figure 7(C-a). The FWHM of the ASE spectra decreases sharply from 2 μJ to 4 μJ and becomes approximately uniform when the pumping energy ranges from 6 μJ and 12 μJ, as shown in Figure 7C-c. Peak stability was examined using the spectra versus excitation energy. The ASE peaks are found to be quite stable and constant with the excitation energy, as displayed in Figure 7C-b. Although the present experiment could exhibit ASE-like spectra, more detailed explanation is needed about such composite rods in terms of ASE parameters, such as the threshold condition of the samples, proper pump energy, different sizes of the samples etc., in order to achieve lasing.



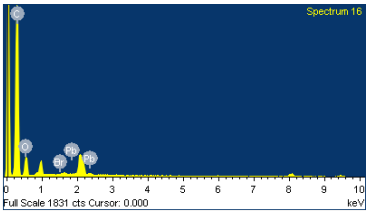
(A)



(B)



(C)



(D)

Fig. 8. SEM images of PQ-Dots in **(A)** solution, **(B and C)** composite polymer rods; **(D)** EDX spectra. EDX, energy dispersive X-ray spectroscopy; PQ-Dots, perovskite quantum dots

3.4. Surface morphology and PQ-Dot sizes

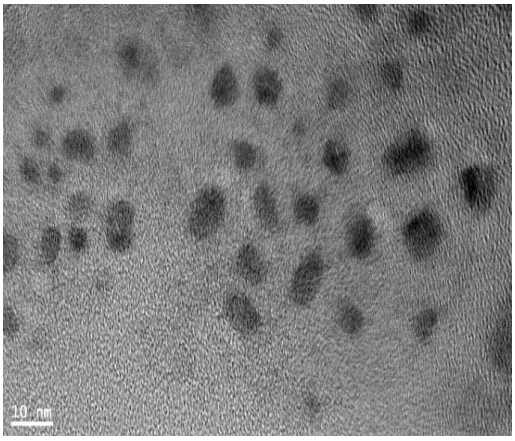
The surface micrograph structure of the PQ-Dot solution and solid composite polymer environment was studied by scanning electron microscopy

(SEM). The micrograph images of the Q-Dots in solution were taken after drying, as shown in Figure 8A. The micrographs of the PQ-Dots in the polymer solid matrix are shown in Figures 8B and 8C. The presence and distribution of the PQ-Dots in solution and solid matrix are shown in Figures 8A and 8B. Distribution of some PQ-Dot particles can be seen in the solid environment when the image is magnified (Figure 8C). It indicates that the distribution of the Q-Dot particles in the solid polymer is uniform. As depicted in Figure 8, agglomerates of PQ-Dots with sizes in the order of hundreds of nanometers are well dispersed in the polymer matrix; the PQ-Dots are uniformly dispersed inside the agglomerates (Figure 9) and uniformly spread in the form of clusters. In addition, a significant presence of the Q-Dot particles on the polymer surface is confirmed by the EDX spectra, as shown in Figure 8D.

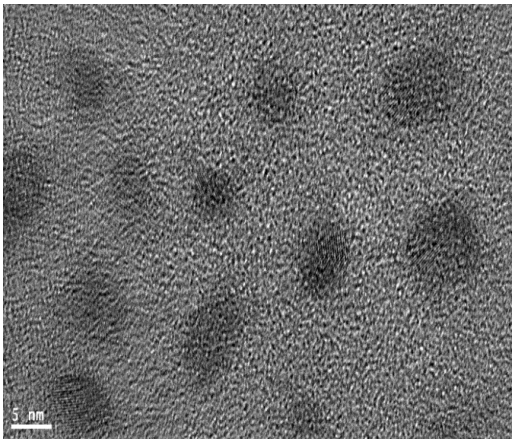
The size of PQ-Dots in solution and the solid environment is inspected by a TEM. TEM images of the Q-Dots in solution at high and low resolution were collected to identify the particle size and crystalline structure. The distribution of different sizes within the crystalline structures is displayed in Figure 9A. Majority of the Q-Dots are in the range of 3–8 nm in size and are roughly spherical in shape.

The crystalline nature of the Q-Dots in solution is seen in the high-resolution image shown in Figure 9B. The energy dispersive X-ray spectroscopy (EDX) spectra indicate the presence of Pb and Br in the solution (Figure 9C). Similarly, the TEM images of the PQ-Dot particles in the solid polymer environment at low and high resolutions are shown in Figures 10A and 10B. There is no aggregate of PQ-Dot particles in the composite.

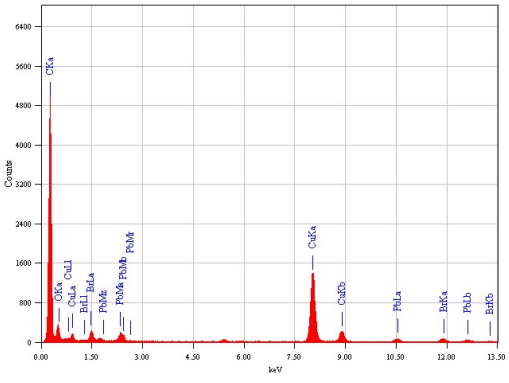
A significant number of PQ-Dots are observed in the solid matrix. A clear crystalline structure of the PQ-Dots in the solid matrix is seen in Figure 10B. The EDX spectra of the PQ-Dots show the existence of Q-Dots in the solid environment, as seen in Figure 10C. The existence and dispersal of PQ-Dots in the solid composite may be attributed to the polymer matrix, which preserves the dopant during the solidification of the matrix.



(A)

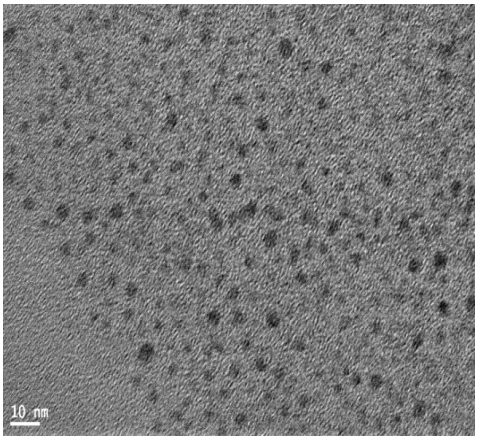


(B)

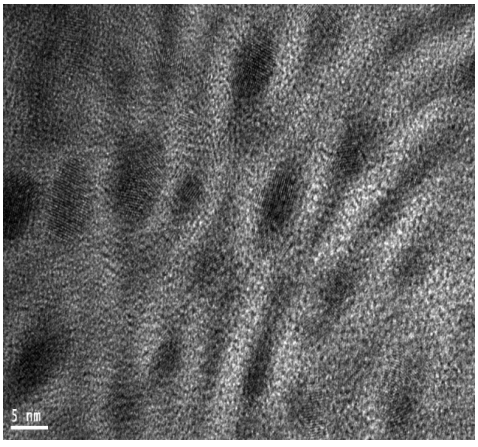


(C)

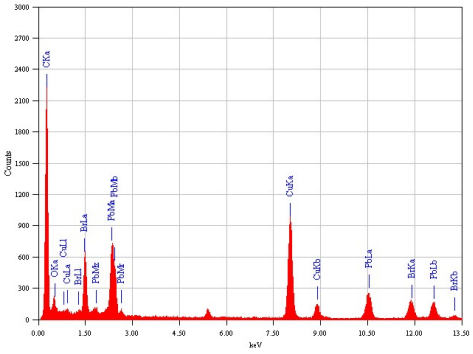
Fig. 9. TEM images of PQ-Dots at **(A)** low and **(B)** high resolution; **(C)** EDX spectra. EDX, energy dispersive X-ray spectroscopy; PQ-Dots, perovskite quantum dots



(A)



(B)



(C)

Fig. 10. TEM images of the PQ-Dot composite polymer matrix at **(A)** low and **(B)** high resolution; **(C)** EDX spectra. EDX, energy dispersive X-ray spectroscopy; PQ-Dots, perovskite quantum dots

4. Conclusions

The PQ-Dot solution was directly incorporated in a polymer sol and used to successfully fabricate solid composite rods and disks. The final product was found to be stable without harming the PQ-Dots. The micrograph structure showed the presence of the PQ-Dot particles, which were confirmed by EDX. Some of the PQ-Dots were agglomerated in the matrix surface. The particle size was found to be in the range of about 3–8 nm. The composite rods were easily cut into different sizes, and then their optical and spontaneous emission properties were studied. The optical properties of the PQ-Dots in the solid matrix were not degraded or negatively affected. The observed emission and spontaneous emission properties of the PQ-Dots in the solid-polymer matrix were not much changed from the relative emission properties of the PQ-Dot solution. ASE-like spectra were observed with the shorter rod, and this effect was achieved at low excitation energy. The ASE peak of the PQ-Dot in the solid environment was not influenced by the pumping of different excitation energies. The stability of the PQ-Dots in the polymer rod indicates that it may further improve from ASE to lasing in the future. It is recommended that future studies should focus on achieving ASE, which may transform the PQ-Dot composite-based lasers. Such composite rod or disk samples can maintain the PL stability of the PQ-Dots by protecting them from oxides and humid environments, which is a key issue in their applications. Further study on higher concentrations and different sizes of composite rods are under way for developing their applications from ASE to lasing.

Acknowledgements

The authors would like to thank the Deanship of Scientific Research at the Islamic University of Madinah, Saudi Arabia, for the financial support of this work through the program Tamayuz 11 of the academic year 2020/2021, research project No. 244. The authors also extend thanks to Laser and Spectroscopy Lab, King Abdullah Institute for Nanotechnology, for their help in carrying out the experimental works.

References

[1] Murawski C, Leo K, Gather MC. Efficiency roll-off in organic light-emitting diodes. Adv Mater.

2013;25:6801. https://doi.org/10.1002/adma.201301603

[2] Burroughes JH, Bradley DDC, Brown AR, Marks RN, Mackay K, Friend RH, et al. Light-emitting diodes based on conjugated polymers. Nature. 1990;347:539. https://doi.org/10.1038/347539a0

[3] Coe S, Woo WK, Bawendi M, BulovicV. Electroluminescence from single monolayers of nanocrystals in molecular organic devices. Nature. 2002;420:800. https://doi.org/10.1038/nature01217

[4] Alivisatos AP. Semiconductor clusters, nanocrystals, and quantum dots. Science. 1996;271(5251):933. https://doi.org/10.1126/science.271.5251.933

[5] Shirasaki Y, Supran GJ, Bawendi MG, Bulovic V. Emergence of colloidal quantum-dot light-emitting technologies. Nat Photonics. 2013;7:13. https://doi.org/10.1038/nphoton.2012.328

[6] Sjoerd AV, Pablo PB, Natalia Y, Mingjie L, Tze CS, Nripan M, et al. Perovskite materials for light-emitting diodes and lasers. Adv Mater. 2016;28(22):6804–34. https://doi.org/10.1002/adma.201600669

[7] Xing G, Mathews N, Lim SS, Yantara N, Liu X, Sabba D, et al. Low-temperature solution-processed wavelength-tunable perovskites for lasing. Nat Mater. 2014;13:476–80. https://doi.org/10.1038/nmat3911

[8] Stranks SD, Eperon GE, Grancini G, Menelaou C, Alcocer MJP, Leijtens T, et al. Electron-hole diffusion lengths exceeding 1 micrometer in an organometal trihalide perovskite absorber. Science. 2013;342:341. https://doi.org/10.1126/science.1243982

[9] Tan ZK, Moghaddam RS, Lai ML, Docampo P, Higler R, Deschler F, et al. Bright light- emitting diodes based on organometal halide perovskite. Nat Nanotechnol 2014;9(9):687-92. https://doi.org/10.1038/nnano.2014.149

[10] Li G, Rivarola FWR, Davis Nathaniel JLK, Bai S, Jellicoe TC, de la Penã F, et al. Highly efficient perovskite nanocrystal light-emitting diodes enabled by a universal crosslinking method. Adv Mater. 2016;28(18):3528-34. https://doi.org/10.1002/adma.201600064

[11] Cho H, Jeong SH, Park MH, Kim YH, Wolf C, Lee CL, et al. Overcoming the electroluminescence efficiency limitations of perovskite light-emitting diodes. Science. 2015;350(6265):1222. https://doi.org/10.1126/science.aad1818

[12] Li C, Lu X, Ding W, Feng L, Gao Y, Guo Z. Formability of ABX_3 (X=F,Cl, Br, I) halide perovskites. Acta Crystallogr Sect B Struct Sci. 2008;64:702. https://doi.org/10.1107/S0108768108032734

[13] Green MA, Ho-Baillie A, Snaith HJ. The emergence of perovskite solar cells. Nat Photonics. 2014;8:506. https://doi.org/10.1038/nphoton.2014.134

[14] Kieslich G, Sun S, Cheetham AK. Solid-state principles applied to organic-inorganic perovskites: new tricks for an old dog. Chem Sci. 2014;5:4712–15. https://doi.org/10.1039/C4SC02211D

[15] Lee JW, Kim DH, Kim HS, Seo SW, Cho SM, Park, NG. Formamidinium and cesium hybridization for photo- and moisture-stable perovskite solar cell. Adv Energy Mater. 2015;5. https://doi.org/10.1002/aenm.201501310

[16] Giles EE, Daniel B, Joel T, Samuel DS, Michael BJ, Trystan W, et al. Efficient, semitransparent neutral-colored solar cells based on microstructured formamidinium lead trihalide perovskite. J Phys Chem Lett. 2015;6(1):129–38. https://doi.org/10.1021/jz502367k

[17] Mitzi DB, Field CA, Schlesinger Z, Laibowitz RB. Transport, optical, and magnetic properties of the conducting halide perovskite $CH_3NH_3SnI_3$. J Solid State Chem. 1995;114:159-63. https://doi.org/10.1006/jssc.1995.1023

[18] Chondroudis K, Mitzi DB. Electroluminescence from an organic-inorganic perovskite incorporating a quaterthiophene dye within lead halide perovskite layers. Chem Mater. 1999;11:3028-30. https://doi.org/10.1021/cm990561t

[19] Pedesseau L. et al. Electronic properties of 2D and 3D hybrid organic/inorganic perovskites for optoelectronic and photovoltaic applications. Opt Quantum Electron. 2014;46;1225–32. https://doi.org/10.1007/s11082-013-9823-9

[20] Kumawat NK, Dey A, Kumar A, Gopinathan SP, Narasimhan K.L, Kabra D. Band gap tuning of $CH_3NH_3Pb(Br_{1-x}Cl_x)_3$ hybrid perovskite for blue electroluminescence. ACS Appl Mater Interfaces. 2015;7:13119. https://doi.org/10.1021/acsami.5b02159

[21] Eperon GE, Stranks SD, Menelaou C, Johnston MB, Herz LM, Snaith HJ. Formamidinium lead trihalide: a broadly tunable perovskite for efficient planar heterojunction solar cells. Energy Environ Sci. 2014;7:982–8. https://doi.org/10.1039/C3EE43822H

[22] Noh JH, Im SH, Heo JH, Mandal TN, Seok SI. Chemical management for colorful, efficient, and stable inorganic–organic hybrid nanostructured solar cells. Nano Lett. 2013;13:1764–9. https://doi.org/10.1021/nl400349b

[23] Hao F, Stoumpos CC, Chang RPH, Kanatzidis MG. Anomalous band gap behavior in mixed sn and Pb perovskites enables broadening of absorption spectrum in solar cells. J Am Chem Soc. 2014;136:8094. https://doi.org/10.1021/ja5033259

[24] Ogomi Y, Morita A, Tsukamoto S, Satiro T, Fujiyama N, Shen Q, et al. $CH_3NH_3Sn_xPb_{(1--x)}I_3$ perovskite solar cells covering up to 1060 nm. J Phys Chem Lett. 2014;5:1004–11. https://doi.org/10.1021/jz5002117

[25] Era M, Morimoto S, Tsutsui T, Saito S. Organic-inorganic heterostructure electroluminescent device using a layered perovskite semiconductor $(C_6H_5C_2H_4NH_3)_2PbI_4$. Appl Phys Lett. 1994;65:676.

https://doi.org/10.1063/1.112265

[26] Hong X, Ishihara T, Nurmikko AV. Photoconductivity and electroluminescence in lead iodide based natural quantum well structures. Solid State Commun. 1992;84:657. https://doi.org/10.1016/0038-1098(92)90210-Z

[27] Hattori T, Taira T, Era M, Tsutsui T, Saito S. Highly efficient electroluminescence from a heterostructure device combined with emissive layered-perovskite and an electron-transporting organic compound. Chem Phys Lett. 1996;254:103–8. https://doi.org/10.1016/0009-2614(96)00310-7

[28] Kondo T, Azuma T, Yuasa T, Ito R. Biexciton lasing in the layered perovskite-type material $(C_6H_{13}NH_3)_2PbI_4$. Solid State Commun. 1998;105:253–5. https://doi.org/10.1016/S0038-1098(97)10085-0

[29] Wang J, Wang N, Jin Y, Si J, Tan ZK, Du H, et al. Interfacial control toward efficient and low-voltage perovskite light- emitting diodes. Adv Mater. 2015;27(14):2311-6. https://doi.org/10.1002/adma.201405217

[30] Michael ML, Joël T, Tsutomu M, Takurou NM, Henry JS. Efficient hybrid solar cells based on Meso-Superstructured Organometal Halide Perovskites. Science. 2012;80. https://doi.org/10.1126/science.1228604

[31] Chen S, Roh K, Lee J, Chong WK, Lu Y, Mathews N. et al. A photonic crystal laser from solution based organo-lead iodide perovskite thin films. ACS Nano 2016;10;3959–67. https://doi.org/10.1021/acsnano.5b08153

[32] Sutherland BR, Sargent EH. Perovskite photonic sources. Nat Photonics. 2016;10:295–302. https://doi.org/10.1038/nphoton.2016.62

[33] Mitzi DB, Wang S, Field CA, Chess CA, Guloy AM. Conducting layered organic-inorganic halides containing <110>oriented perovskite sheets. Science. 1995;80:267(5203):1473–6. https://doi.org/10.1126/science.267.5203.1473

[34] Young HK et al. Multicolored organic/inorganic hybrid perovskite light emitting diodes. Adv Mater. 2015;27(7):1248–54. https://doi.org/10.1002/adma.201403751

[35] Wei T, Huanping Z, Liang L. Hybrid organic-inorganic perovskite photodetectors. Small. 2017;41:1702107. https://doi.org/10.1002/smll.201702107

[36] Dou L, Yang Y, You J, Hong Z, Chang WH, Li G, et al. Solution-processed hybrid perovskite photodetectors with high detectivity. Nat Commun. 2014;5:5404. https://doi.org/10.1038/ncomms6404

[37] Zhuo S, Zhang J., Shi Y, Huang Y, Zhang B. Self-template-directed synthesis of porous perovskite nanowires at room temperature for high-performance visible-light photodetectors. Angew Chem Int Ed. 2015;54:5693. https://doi.org/10.1002/anie.201411956

[38] Maculan G, Sheikh AD, Abdelhady A, Saidaminov MI, Haque MA, Murali B, et al. $CH_3NH_3PbCl_3$ single crystals: inverse temperature crystallization and visible-blind UV-photodetector. J Phys Chem Lett. 2015;6:3781–6. https://doi.org/10.1021/acs.jpclett.5b01666

[39] Deschler F, Price M, Pathak S, Klintberg LE, Jarausch DD, Higler R, et al.. High photoluminescence efficiency and optically pumped lasing in solution-processed mixed halide perovskite semiconductors. J Phys Chem Lett. 2014;5:1421. https://doi.org/10.1021/jz5005285

[40] Saif MHQ, Khan MN, Alqasem A, Hezam M, Aldwayyan AA. Restraining effect of film thickness on the behavior of amplified spontaneous emission from methylammonium lead iodide perovskite. IET Optoelectronics. 2018;13(1):2–6. https://doi.org/10.1049/iet-opt.2018.5035

[41] Zhu, H., et al. Lead halide perovskite nanowire lasers with low lasing thresholds and high quality factors. Nat Mater. 2015;14:636–42. https://doi.org/10.1038/nmat4271

[42] Qing Z, et al., Advances in small perovskite based lasers. Small Methods. 2017;1(9):1700163. https://doi.org/10.1002/smtd.201700163

[43] Sutherland BR, Hoogland S, Adachi MM, Wong CT, Sargent EH. Conformal organohalide perovskites enable lasing on spherical resonators. ACS Nano. 2014;8(10):10947–52. https://doi.org/10.1021/nn504856g

[44] Stranks SD, Wood SM, Wojciechowski K, Deschler F, Saliba M, Khandelwal H, et al. Enhanced amplified spontaneous emission in perovskites using a flexible cholesteric liquid crystal reflector. Nano Lett. 2015;15(8):4935–41. https://doi.org/10.1021/acs.nanolett.5b00678

[45] Zhang Q, Ha ST, Liu X, Sum TC, Xiong Q. Room-temperature near-infrared high-Q perovskite whispering-gallery planar nanolasers. Nano Lett. 2014;14:5995. https://doi.org/10.1021/nl503057g

[46] Dhanker R., et al. Random lasing in organo-lead halide perovskite microcrystal networks. Appl Phys Lett. 2014;105:151112. https://doi.org/10.1063/1.4898703

[47] Saliba M, Wood SM, Patel JB, Nayak PK, Huang J, Alexander-Webber JA, et al. Structured organic-inorganic perovskite toward a distributed feedback laser. Adv Mater. 2016;28:923–8. https://doi.org/10.1002/adma.201502608

[48] Liao Q, Hu K, Zhang HH, Wang XD, Yao JN, Fu HB. Perovskite microdisk microlasers self-assembled from solution. Adv Mater. 2015;27(24):3405. https://doi.org/10.1002/adma.201500449

[49] Chen J, Zhou S, Jin S, Li H, Zhai T, Gaál R, et al. Crystal organometal halide perovskites with promising optoelectronic applications. J Mater Chem C. 2016;4:11–27. https://doi.org/10.1039/C5TC03417E

[50] Audebert P, Clavier G, Alain-Rizzo V, Deleporte E,

Zhang S, Lauret JSB, et al. Synthesis of new perovskite luminescent nanoparticles in the visible range. Chem Mater. 2009;21:210–14. https://doi.org/10.1021/cm8020462

[51] Protesescu L, Yakunin S, Bodnarchuk MI, Krieg F, Caputo R, Hendon CH, et al. Nanocrystals of cesium lead halide perovskites ($CsPbX_3$, X = Cl, Br, and I): novel optoelectronic materials showing bright emission with wide color gamut. Nano Lett. 2015;15:3692-6. https://doi.org/10.1021/nl5048779

[52] Wang Y, Zhi M, Chang YQ, Zhang JP, Chan Y. Stable, ultralow threshold amplified spontaneous emission from $CsPbBr_3$ nanoparticles exhibiting Trion gain. Nano Lett. 2018;18:4976-84. https://doi.org/10.1021/acs.nanolett.8b01817

[53] Yakunin S, Protesescu L, Krieg F, Bodnarchuk MI, Nedelcu G, Humer M, et al. Low-threshold amplified spontaneous emission and lasing from colloidal nanocrystals of caesium lead halide perovskites. Nat Commun. 2015;6:8056. https://doi.org/10.1038/ncomms9056

[54] De Giorgi ML, Krieg F, Kovalenko MV, Anni M. Amplified spontaneous emission threshold reduction and operational stability improvement in $CsPbBr_3$ nanocrystals films by hydrophobic functionalization of the substrate. Sci Rep. 2019;9:17964. https://doi.org/10.1038/s41598-019-54412-7

[55] Cho C, Palatnik A, Sudzius M, Grodofzig R, Nehm F, Leo K. Controlling and optimizing amplified spontaneous emission in perovskite. ACS Appl Mater Interfaces. 2020;12(31):35242–9. https://doi.org/10.1021/acsami.0c08870

[56] Leyden MR, Matsushim T, Qin Ch, Ruan S, Ye H, Adachi C. Amplified spontaneous emission in phenylethylammonium methylammonium lead iodide quasi-2D perovskites. Phys Chem Chem Phys. 2018;20:15030–6. https://doi.org/10.1039/C8CP02133C

[57] Aleksei OM, Stroganov BV, Günnemann C, Hammouda SB, Shurukhina AV, Lozhkin MS. et al. Amplified spontaneous emission and random lasing in MAPbBr3 halide perovskite single crystals. Adv Optical Mater. 2020;8(17):2000690. https://doi.org/10.1002/adom.202000690

[58] Zhang Q, Su R, Liu X, Xing J, Sum TC, Xiong Q. High-quality whispering-gallery-mode lasing from cesium lead halide perovskite nanoplatelets. Adv Funct Mater. 2016;26:6238-45. https://doi.org/10.1002/adfm.201601690

[59] Liu S, Sun W, Li J, Gu Z, Wangm K, Xiao S, et al. Random lasing actions in self-assembled perovskite nanoparticles. Opt Eng. 2016;55(5):057102. https://doi.org/10.1117/1.0E.55.5.057102

[60] Saif MHQ, Al-Asbahi BA, Ghaithan HH, Alsalhi MS, Aldwayyan AS. Optical and structural properties of $CsPbBr_3$ perovskite quantum dots/PFO polymer composite thin films. J Colloid Interface Sci. 2020;563:426–34. https://doi.org/10.1016/j.jcis.2019.12.094

[61] Wang Y, Xiaoming Li, Song J, Xiao L, Zeng H, Sun H. All-inorganic colloidal perovskite quantum dots: A new class of lasing materials with favorable characteristics. Adv Mater. 2015;27:7101–8. https://doi.org/10.1002/adma.201503573

[62] Ning Z, Gong X, Comin R, Walters G, Fan F, Voznyy O, et al. Quantum-dot-in-perovskite solids. Nature. 2015;324(523):2015. https://doi.org/10.1038/nature14563

[63] Sun C, Zhang Y, Ruan C., et al. Efficient and stable white LEDs with silica-coated inorganic perovskite quantum dots. Adv Mater. 2016;28(45):10088–94. https://doi.org/10.1002/adma.201603081

[64] Wei Y, Xiao H, Xie Z., et al. Highly luminescent lead halide perovskite quantum dots in hierarchical CaF_2 matrices with enhanced stability as phosphors for white light-emitting diodes. Adv Opt Mater. 2018;6(11):1701343. https://doi.org/10.1002/adom.201701343

[65] Yang G, Fan Q, Chen B, et al. Reprecipitation synthesis of luminescent $CH_3NH_3PbBr_3/NaNO_3$ nano- composites with enhanced stability. J Mater Chem C. 2016;4(48):11387–91. https://doi.org/10.1039/C6TC04069A

[66] Pang X, Zhang H, Xie L, et al. Precipitating $CsPbBr_3$ quantum dots in boro-germanate glass with a dense structure and inert environment toward highly stable and efficient narrow-band green emitters for wide-color-gamut liquid crystal displays. J Mater Chem C. 2019;7(42):13139–48. https://doi.org/10.1039/C9TC04732H

[67] Pan J, Sarmah SP, Murali B, Dursun I, Peng W, Parida MR, et al. Air-stable surface-passivated perovskite quantum dots for ultra-robust, single- and two-photon- induced amplified spontaneous emission. J Phys Chem Lett. 2015;6:5027-33. https://doi.org/10.1021/acs.jpclett.5b02460

[68] Xiong Q, Huang S, Du J, Tang X, Zeng F, Liu Z, et al. surface ligand engineering for $CsPbBr_3$ quantum dots aiming at aggregation suppression and amplified spontaneous emission improvement. Adv Opt Mater. 2020;8:2000977. https://doi.org/10.1002/adom.202000977

[69] Moon H, Lee C, Lee W, et al. Stability of quantum dots, quantum dot films, and quantum dot light-emitting diodes for display applications. Adv Mater. 2019;31(34):1804294. https://doi.org/10.1002/adma.201804294

[70] Yang J, Siempelkamp BD, Liu D., et al. Investigation of $CH_3NH_3PbI_3$ degradation rates and mechanisms in controlled humidity environments using in situ techniques. ACS Nano. 2015;9(2):1955–63. https://doi.org/10.1021/nn506864k

[71] Christians JA, Miranda HPA, Kamat PV. Transformation of the excited state and photovoltaic efficiency of

CH3NH3PbI3 perovskite upon controlled exposure to humidified air. J Am Chem Soc 2015;137(4);1530–8. https://doi.org/10.1021/ja511132a

[72] Palazon F, Di SF, Lauciello S, et al. Evolution of $CsPbBr_3$ nanocrystals upon post-synthesis annealing under an inert atmosphere. J Mater Chem C. 2016;4(39):9179–82. https://doi.org/10.1039/C6TC03342C

[73] Huang S, Li Z, Wang B, et al. Morphology evolution and degradation of $CH_3NH_3PbI_3$ nanocrystals under blue light-emitting diode illumination. ACS Appl Mater Interfaces. 2017;9(8);7249–58. https://doi.org/10.1021/acsami.6b14423

[74] Gong Y, Shen J, Zhu Y, Yang X, Zhang L, Li C. Stretch induced photoluminescence enhanced perovskite quantum dot polymer composites. J Mater Chem C. 2020;8:1413–20. https://doi.org/10.1039/C9TC05966K

[75] Chen LC, Tien CH, Tseng ZL, Dong YS, Yang S. Influence of PMMA on all inorganic halide perovskite $CsPbBr_3$ quantum dots combined with polymer matrix. Materials. 2019;12:985. https://doi.org/10.3390/ma12060985

[76] Khan MN, Al Dwayyan AS, Al Salhi MS. Study on characteristics of silicon nanocrystals within sol-gel host. J Exp Nanosci. 2012;7(2):120. https://doi.org/10.1080/17458080.2010.513016

[77] Khan MN, Al Dwayyan AS. Influence on structural and PL property of nanocrystals silicon doped sol gel matrix. J Optoelectron Adv Mater. 2012;14(5):448.

[78] Khan MN, Al Dwayyan AS, Al Hossain MS. Morphology and optical properties of a porous silicon-doped sol-gel host. Electron Mater Lett. 2013;9(5):697. https://doi.org/10.1080/17458080.2010.513016

[79] Khan MN, Aldalbahi A, Almohamedi A. Investigation of different colloidal porous silicon solutions and their composite solid matrix rods by optical techniques. J Electron Mater. 2018;47(7):3596–607. https://doi.org/10.1007/s11664-018-6204-y

[80] Khan MN, Aldalbahi A, Al Dwayyan AS. Composite rods based on nanoscale porous silicon in sol–gel silica and ormosil matrices for light-emitting applications. J Sol-Gel Sci Technol. 2017;82:551–62. https://doi.org/10.1007/s10971-017-4309-z

[81] Khan MN, Al Dwayyan AS, Aldalbahi A. Light emitting composite rods based on porous silicon in ormosils and polymer matrices for optical applications. Opt Laser Technol. 2017;91:203–11. https://doi.org/10.1016/j.optlastec.2016.12.035

Received 2021-12-09
Accepted 2022-04-11